PAPER

Delicate superconductivity in nodal-line NaAlGe single crystal

IOP Publishing Journal of Physics: Condensed Matter
J. Phys.: Condens. Matter **34** (2022) 495702 (8pp) https://doi.org/10.1088/1361-648X/ac9adf

Delicate superconductivity in nodal-line NaAlGe single crystal

Zhaoxu Chen[1,2], Yuxin Yang[1,3], Jun Deng[1], Shixuan Du[1], Tianping Ying[1,*], Jiangang Guo[1,4,*] and Xiaolong Chen[1,4]

[1] Beijing National Laboratory for Condensed Matter Physics, Institute of Physics, Chinese Academy of Sciences, Beijing 100190, People's Republic of China
[2] School of Physical Sciences, University of Chinese Academy of Sciences, Beijing 100049, People's Republic of China
[3] College of Materials Sciences and Opto-Electronic Technology, University of Chinese Academy of Sciences, Beijing 100049, People's Republic of China
[4] Songshan Lake Materials Laboratory, Dongguan 523808, People's Republic of China

E-mail: ying@iphy.ac.cn and jgguo@iphy.ac.cn

Received 20 July 2022, revised 30 September 2022
Accepted for publication 17 October 2022
Published 26 October 2022

Abstract

Nodal-line superconductor NaAlSi with a transition temperature (T_c) of 7 K has attracted considerable attention in recent years, whereas its Ge counterpart, NaAlGe, does not superconduct down to the lowest temperature regardless of their similar atomic and electrical structures. To tackle this enigma, we resort to the growth of NaAlGe single crystal and characterize its ground state. Interestingly, when hole doped by oxidation or extracting Na, single-crystalline NaAlGe transforms from a semimetal/semiconductor to a superconductor ($T_c = 1.8 \sim 3.3$ K) with zero resistivity and a diamagnetic shielding fraction over 100%, but without a thermodynamic response in heat capacity. Continuous x-ray diffraction reveals a transient new structure with a larger c axis, which is suggested to have arisen from the minor loss of Na and to be responsible for the emergence of the delicate superconductivity. Our findings place NaAlGe on an equal footing with NaAlSi and provide an alternative for studying the intriguing relationship between superconductivity and nodal-line topology.

Keywords: superconductivity, nodal-line, topological material

(Some figures may appear in colour only in the online journal)

1. Introduction

Topological semimetals are materials in which the conduction and the valence bands cross each other and all bands are protected by symmetries. When the band crossing run across the Brillouin Zone or wind into one closed loop or several connected loops, the material is sorted as a nodal line semimetal [1]. These nodal lines are intrinsically related to a two-dimensional (2D) drumhead-like topological surface that resembles the edge states in nodal-point materials and holds the promise of realizing a series of magnetoelectric and electrical-transport properties [2–4]. In the framework of BCS theory, superconductors generally require a high density of states at the E_F, so nodal states are thought to be more favorable to harbor a higher transition temperature. The widely investigated prototype is $PbTaSe_2$ with its topological properties protected by the reflection symmetry and the breaking of space inversion symmetry [5–7]. However, due to the existence of trivial bands near the Fermi level (E_F), whether the superconductivity is derived from its topological nature is still under debate [8, 9].

* Authors to whom any correspondence should be addressed.

NaAlSi has recently been discovered to be a new kind of nodal-line superconductor ($T_c = 7$ K) [10, 11], in which all the bands involving nodal rings lie near the E_F without mixing with other trivial ones [12–15]. NaAlSi crystallized in an anti-PbFCl layer structure with a space group of No. 129 $P4/nmm$ [10], isostructural to LiFeAs [16] and LiFeP [17]. Al-Si is tetrahedrally coordinated and edge shared to form a quasi-2D layer, stacking along the c-axis with Na atoms in between. Theoretical calculations show multiple nodal lines in the vicinity of E_F with the bands composed of a mixture of electrons from both Al and Si [12–14]. The drumhead Fermi surface is contributed by the hole-like Si-3p orbitals with nearly flat band dispersion and heavy electron effective mass, while the light electron bands mainly come from Al-3s orbitals [18]. The drumhead Fermi surfaces are suggested to be responsible for the intrinsic transport properties [11], whereas the correspondence between superconductivity and topology is not clear. Intensive enthusiasms have been devoted to the research of NaAlSi recently. Muon spin relaxation experiments confirmed the bulk superconductivity with a full gap opening [14]. Its T_c can be increased to 9 K under external pressure [19]. Furthermore, a fractional superconducting signal has been observed on the surface of the single crystals aside from its bulk superconductivity [20].

It has long been known that NaAlSi has a sister compound NaAlGe by replacing Si for Ge [10]. However, the powder form of NaAlGe does not show any trace of superconductivity down to the lowest temperature [10] and its underlying mechanism is poorly understood [18]. The band structures of both compounds are quite similar, except for a missing piece of a small electron pocket on the α band along the $\mathbf{\Gamma} - M$ direction in NaAlGe [18]. It has been suggested that the missing electron pocket is crucial for the absence of superconductivity in NaAlGe and is highly sensitive to the z-coordinate of Si in NaAlSi. Other scenarios such as stronger electron-phonon coupling strength arising from the lighter Si or different electron pairing mechanism have been suggested [18]. On the other hand, all the nodal lines are located slightly below E_F [21]. Nontrivial phenomena can thus be anticipated if the system could be hole-doped to shift the Fermi level approaching the crossing sections.

In this paper, we report the successful synthesis of NaAlGe single crystal, following the recent growth of NaAlSi single crystal by Na-Ga flux [11, 20]. The physical properties of NaAlGe single crystals are studied by electrical resistivity, magnetization, and heat capacity measurement. Despite the intrinsic semimetallic/semiconducting ground state, NaAlGe single crystal shows a distinct superconducting transition with the T_c varies from 1.8 K to 3.3 K and a perfect diamagnetic response over 100%. Detailed characterizations reveal that the observed superconductivity is not a bulk response, but corresponds to a hole-doped $Na_{1-\delta}AlGe$ with a slightly elongated c axis. A conceptional illustration of a sandwich structure is given to explain all the observed phenomena. Our findings suggest that NaAlGe is an interesting platform to study the relationship between hole-doping induced superconductivity and topology [22–24].

2. Experimental

Powder crystals of NaAlGe were synthesized with Na lump, Al powder, and Ge powder as starting materials. The starting materials were weighted to a molar ratio of Na:Al:Ge = 1:1:1. The Al powder and Ge powder were well mixed and pressed into a pellet and loaded into alumina crucibles together with Na. The alumina crucibles covered with a cap were arc-sealed into steel cubes. We slowly heated these steel cubes to 850 °C, held for 6 h and furnace cooled to room temperature. A second annealing process was necessary to ensure homogeneity.

Single crystals were grown using Na lump, Al rod, Ge ingot, and Ga shot with a molar ratio of Na:Al:Ge:Ga = 3:1:1:0.5. We loaded the raw materials into an alumina crucible covered with a cap and sealed into a steel cube (SUS304). The sample was heated to 850 °C, holding for 24 h and then slowly cooling down to room temperature. To remove the Na-Ga flux, we put the crucible into anhydrous alcohol to remove the flux. Millimeter-size single crystals can be collected from the bottom of the crucible. Because of the highly hygroscopic nature of NaAlGe, all manipulations were performed in the Ar atmosphere. To minimize the degree of oxidation, the anhydrous alcohol was bubbled with argon to remove the trace amount of dissolved oxygen. We note that this washing process will still inevitably introduce surface oxidation. Thus, the intrinsic properties of NaAlGe are collected from the crystals directly pealed off from the flux in a glove box without alcohol treatment. For superconducting samples, hole-doping was realized by exposing the sample to air or soaking in alcohol for a few days.

Powder x-ray diffraction (XRD) measurements were performed on a Panalytical X'pert Diffractometer with a Cu K_α anode (1.5418 Å) at room temperature. The Fullprof software was used for Rietveld refinement [25]. The scanning electron microscopy (SEM) image of the single crystal was captured from the Hitachi S-4800 field emission scanning electron microscope. The element mapping of the sample was determined by the energy dispersive spectroscopy. Transport, magnetic and thermodynamic properties were measured using a Physical Property Measurement System (Quantum Design), Magnetic Property Measurement System (Quantum Design), and Keithley 6221/2182A-based home-made electrical resistivity measurement system.

The density functional theory (DFT) calculations were performed within Vienna *ab initio* simulation Package [26]. We adopted the generalized gradient approximation in the form of Perdew–Burke–Ernzerhof [27] for the exchange-correlation potentials. The projector augmented-wave (PAW) pseudopotentials were used with a plane wave energy of 500 eV; $2p^6 3s^1$ for Na, $3d^{10}4s^2 4p^2$ for Ge, and $3s^2 3p^1$ for Al electron configuration were treated as valence electrons. Monkhorst-Pack [28] Brillouin zone sampling grids with a resolution $0.02 \times 2\pi \cdot$Å^{-1} in the self-consistent calculation and $0.01 \times 2\pi \cdot$Å^{-1} for density of states were applied, respectively. These parameters were chosen when the adjacent energy variation was less than 1 meV/atom by variation of plane-wave energy and k points spacing. The self-consistent field procedure was considered

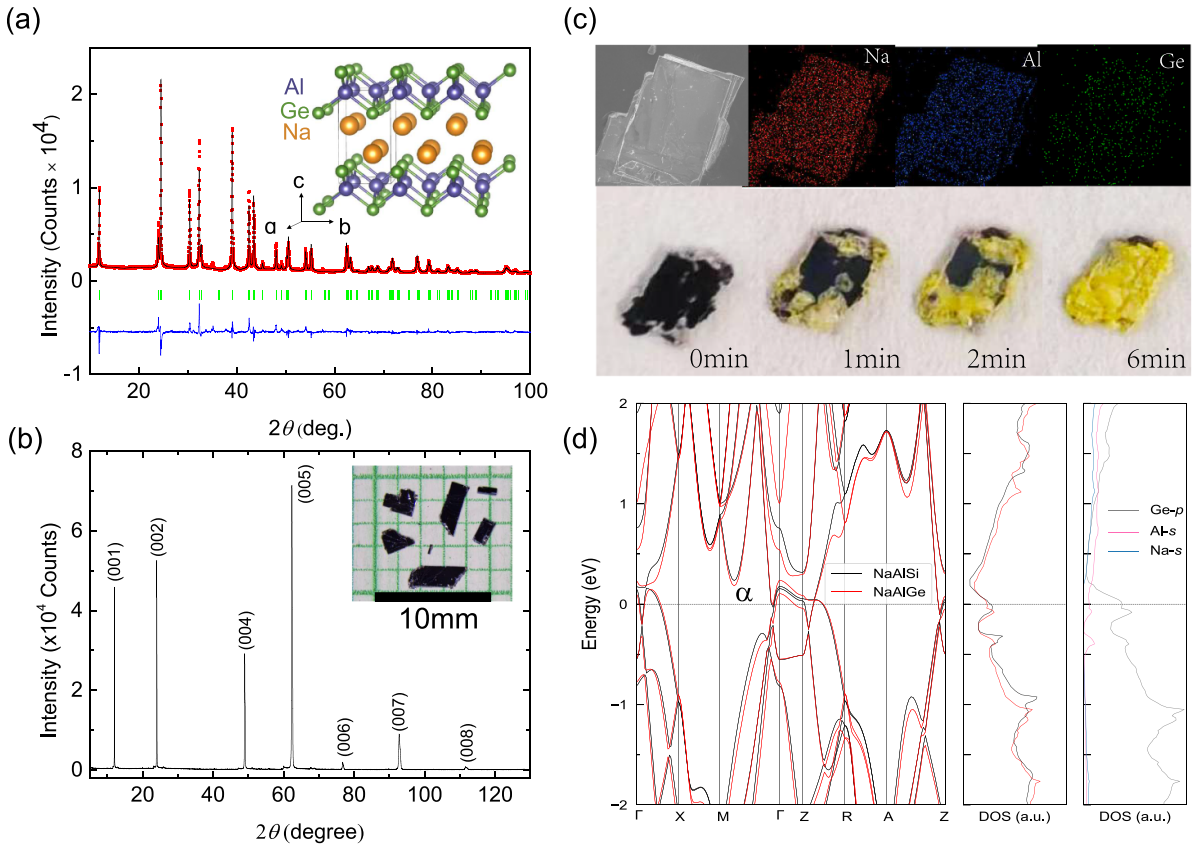

Figure 1. Crystal structure, x-ray diffraction, composition, and electronic structure of NaAlGe. (a) Powder x-ray diffraction of NaAlGe. The red point represents the observed signal, and the black, green, and blue line represent the calculated curve, Bragg positions, and residual difference, respectively. Inset shows its crystal structure. (b) XRD pattern of NaAlGe $(00l)$ plane. Inset is an optical photo of the acquired single crystals. (c) The upper panel is an SEM image of NaAlGe and an EDS mapping of Na (red), Al (blue), and Ge (green). The lower panel displays the morphology of a crystal exposed to air over time. (d) Left: the band of NaAlGe and NaAlSi. Middle: the density of state of NaAlGe and NaAlSi. Right: the projected density of state of NaAlGe.

converged when the energy difference between two consecutive cycles was lower than 10^{-6} eV. The atomic positions and lattice parameters were relaxed until all the forces on them were less than 0.01 eV Å^{-1}. A tiny deficiency in Na site (1% – 3%) is created using virtual crystal approximation, where no mixture of different PAW potentials is used.

3. Results and discussion

The NaAlGe powder was firstly synthesized in 2007 under high pressure [10]. We found that NaAlGe powder can be feasibly synthesized at ambient pressure using steel tubes. Figure 1(a) shows the Rietveld refinement of the powder x-ray diffraction. The refined lattice constants were determined to be $a = b = 4.1591(1)$ Å, $c = 7.4164(2)$ Å, while the reliable factors $R_p = 5.20\%$, $R_{wp} = 7.21\%$, $R_{\rm exp} = 2.69\%$ and $\chi^2 = 7.18$. The inset of figure 1(a) shows the crystal structure of NaAlGe, isostructural to NaAlSi. Figure 1(b) shows the $(00l)$ peak of the NaAlGe single crystal. As shown in the inset, all samples have shining surfaces.

The upper panel of figure 1(c) shows the homogeneous dispersion of Na, Al, and Ge of the sample. Compared to the air-sensitive NaAlSi [11], NaAlGe is much more reactive to moisture and highly hygroscopic. When exposed to air, there is an obvious color change on the crystal surface. As shown in the lower panel of figure 1(c), the crystal surface transforms from silvery white to light yellow and finally orange color. Among the oxides of sodium, which includes Na_2O, Na_2O_2 and NaO_2, only NaO_2 is orange. Na_2O_2 usually looks orange, because of the coexistence of NaO_2 impurity. The color of the final product indicates the existence of NaO_2. Because NaO_2 reacts quickly with H_2O, and then produces Na_2O_2 and NaOH. Considering the sensitivity of NaAlGe to H_2O, Na_2O_2 is also suggested to exist in the final product. Because Al and Ge cannot form a binary compound, Al/Ge oxides possibly form. No peaks appearing on the XRD pattern (see in figure 4(b)) indicates all the final products are amorphous. When reacted with water, both powder and single-crystal will burn or even explode, accompanied by an increase in the pH value of the remaining solvent. Because the Pauling's electronegativity of Si (1.90) is smaller than of Ge (2.01), it seems difficult to understand why NaAlSi is more sensitive than NaAlGe. Considering the atomic radius, Ge (1.365 Å) is larger than Si (1.269 Å), so it is easier to lose valence electrons. Thus, the higher sensitivity of NaAlGe than that of NaAlSi may be a synergistic effect of electronegativity and atomic radius [29].

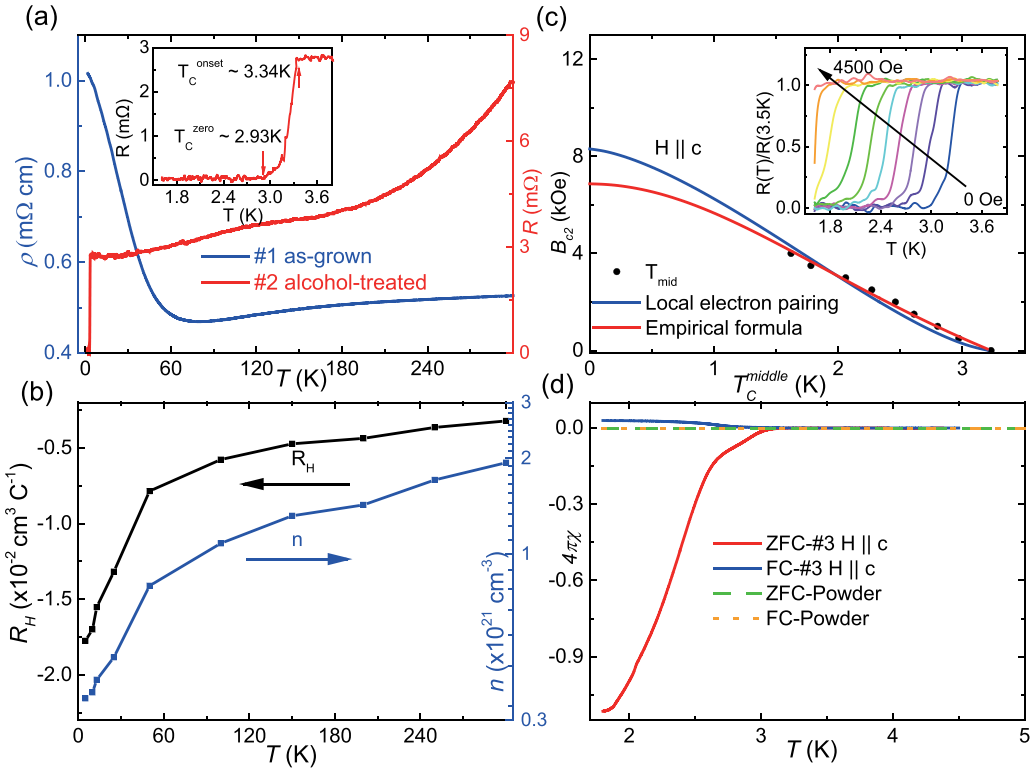

Figure 2. Physical properties of the as-grown NaAlGe and alcohol-treated NaAlGe single crystals. (a) Electrical transport of as-grown NaAlGe (blue) and alcohol-treated NaAlGe (red) single crystals. Inset emphasizes the superconducting transition around 3.3 K. (b) Temperature dependences of Hall coefficient $R_{\rm H}$ and carrier density n of the as-grown NaAlGe. (c) Temperature dependence of the upper critical field $H_{\rm c2}$. The $T_{\rm c}$ is defined at the midpoints of a 50% drop of the normal-state resistance. The blue or red solid line represents the local electron pairing fitting or the empirical formula fitting. Inset shows the temperature-dependent resistance under different magnetic field along the c-axis. (d) Zero-field cooling (ZFC) and field cooling (FC) curves of NaAlGe powder and single crystal were measured under an external field of 10 Oe.

Figure 1(d) presents the electronic structures of NaAlGe and NaAlSi, which are consistent well with the previous reports [12–14, 21]. The Al 3*s* electron bands and the Ge/Si $4p/3p$ heavy hole bands dominate the Fermi surface, while the contribution of Na is small. The main dispersion crossing the Fermi surface happened in the plane, while the band along $\mathbf{\Gamma} - Z$ is rather flat. This suggests the nature of two-dimensionality in NaAlGe. As a result, we find NaAlGe can be easily exfoliated. Detailed investigation of its transport behavior in reduced dimension is underway in our lab. It is worth noting that the electron pocket cannot be observed in the α-band of NaAlSi along the $M - \mathbf{\Gamma}$ path in our calculation, which is previously suggested to may be related to the superconductivity in NaAlSi [18]. Many calculations [12–14] and the recent magnetic torque measurement [30] did not observe this electron pocket, as this pocket is sensitive to the z-coordinate of Si. We suggest that the superconductivity observed in NaAlGe originates from surface-oxidation-induced hole-doping, and will prove the electron pocket along $\mathbf{\Gamma} - M$ is not of great importance (vide infra). The multiple nodal lines can be clearly distinguished slightly 20 meV below the $E_{\rm F}$.

To clarify the ground states of NaAlGe, we scrutinize the electrical transport and the magnetization behavior of NaAlGe single crystal. Due to the sensitivity to moisture, NaAlGe single crystal was carefully handled in the Ar-filled glove box to minimize the oxidation. The in-plane resistivity of the as-grown NaAlGe was shown as blue curve in figure 2(a). At a high temperature, the resistivity increases upon the temperature increases, indicating a metallic behavior. Below ∼75 K, different from the metallic NaAlSi in the whole temperature range, the resistivity of NaAlGe exhibits an anomalous upturn. Hall coefficient and the corresponding carrier density are shown in figure 2(b). There is a linear relationship between the Hall resistance and the magnetic field, which indicates the dominant carrier is electrons from the Al 3*s* band. At room temperature, the carrier density of NaAlGe is 2×10^{21} cm^{-3}, but quickly drops below 50 K and reaches 3×10^{20} cm^{-3} at 5 K. The temperature dependence of carrier density in NaAlSi shows a dome at around 100 K [11], while there is a monotonic increase with temperature in the carrier density of NaAlGe. In the whole temperature range, NaAlGe possessed a smaller carrier density than that of NaAlSi. The drop of carrier density at 50 K is consistent well with the resistivity increase shown in figure 2(a), pointing to the anomaly of resistivity that may originate from the loss of carrier.

The physical properties of NaAlGe can be dramatically altered when alcohol was employed to remove the Na-Ga flux. The electrical transport is shown as the red solid line in figure 2(a), which was totally different from that of the as-grown NaAlGe. The resistance behaves as a metal above

3.35 K. It decreases rapidly above ∼200 K and slowly below 200 K. When cooled to 3.3 K, it undergoes a superconducting transition. The T_c^{zero} is 2.9 K and the transition width is around 0.4 K. To investigate the properties of the superconducting state in alcohol-treated NaAlGe, the magneto transport and magnetization were measured. The resistance at low temperatures under different magnetic fields along the *c*-axis was shown in the inset of figure 2(c). $H_{c2}(T)$ was determined as the midpoint of the superconducting transition and summarized in figure 2(c). To compare with NaAlSi, local electron pairing model [31], $H_{c2}(T) = H_{c2}(0)[1-(T/T_c)^{3/2}]^{3/2}$, was applied and the H_{c2} (0) was fitted to be 6.8 kOe. Furthermore, an empirical formula $\mu_0 H_{c2} = H_{c2}(0)(1-t^2)/(1+t^2)$ gave an upper critical field of 8.3 kOe. Both were much less than Pauli limit 6 T and the $H_{c2}(0)$ of NaAlSi [11]. The coherence length can be acquired from $\mu_0 H_{c2}(0) = \Phi_0/2\pi\xi_0^2$ as 22 nm. Figure 2(d) plots the temperature dependence of the magnetic susceptibility of NaAlGe powder and alcohol-treated NaAlGe in the temperature range from 1.8 K to 5.0 K with a magnetic field along the *c*-axis. Our NaAlGe powder shows no superconductivity, as reported previously [10]. Meanwhile, there are two obvious diamagnetic signals located at 3 K and 2.7 K in the zero-field cooling (ZFC) curve of the alcohol-treated NaAlGe single crystal, indicating the existence of multiple superconducting phases. At 1.8 K, the superconducting volume fraction is estimated to be 110%. The part exceeding 100% mainly come from the diamagnetic shielding effect, incorrect demagnetization factor and the overestimation of molar mass of $Na_{1-\delta}AlGe$ [11, 32, 33].

Heat capacity measurement, a method to analyze the entropy loss during the superconducting transition, is important to ensure the bulk feature [34]. We performed heat capacity measurement on an alcohol-treated NaAlGe with the superconducting transition at 2.6 K that determined by the ZFC curve (figure 3(a)). Although the superconducting volume fraction exceeded 100% in magnetic susceptibility, no jump was observed on $C_p/T \sim T^2$ curve at the corresponding transition temperature, which has also been observed in $Ni_{0.04}ZrTe_2$ [35]. By a fit of the conventional Debye model, the electron coefficient $\gamma = 4.93$ mJ mol^{-1} K^2 and the Debye temperature $\Theta_D = 241.12$ K. Notably, there was a deviation from the linear relationship below 5 K in heat capacity, whose origin was not clear. The heat capacity indicates that the superconductivity should not be bulk form. In order to clarify the origin of superconductivity, the evolution of temperature-dependent resistance versus time was investigated. As mentioned above, the resistance undergoes a metal-semiconductor-like transition at about 50 K. We noticed that even for the as-grown crystal not being treated with alcohol, NaAlGe still undergoes a superconducting transition at low temperature after a slight explosion to air, as shown in figure 3(b). The superconductivity of the same crystal will gradually vanish over a long exposure time.

Inspired by the selective surface oxidation which introduces hole doping in CsV_3Sb_5 [22] and the layered structure of NaAlGe, a hole-doping induced superconducting layer model was proposed. As shown in figure 4(a), the as-grown NaAlGe

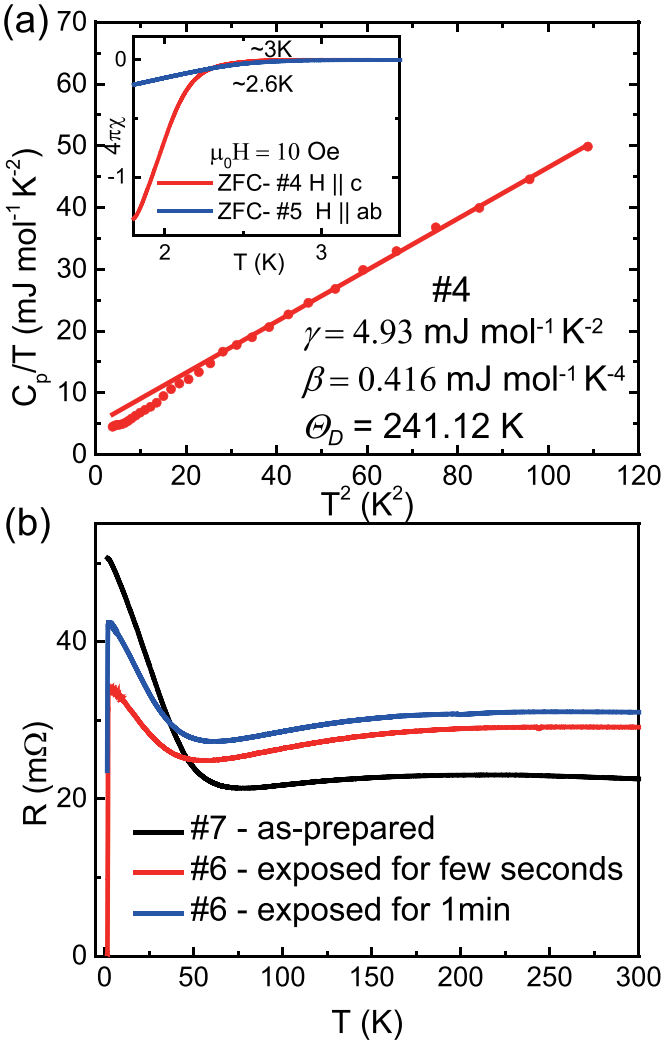

Figure 3. (a) C_p/T versus T^2 plot. The red solid line represents the conventional Debye model fitting. Inset shows the ZFC curve under a magnetic field of 10 Oe within the *ab* plane and along the *c*-axis. (c) Temperature dependence resistance with different exposure time in the air.

is non-superconducting. When exposed to air or trace water in the alcohol, the surface will be quickly over-doped. But the inside a few layers become hole-doped with a suitable doping content. Due to the electromagnetic shielding effect, once two layers become superconducting, the remaining layers in between will exhibit an over-estimated superconducting diamagnetism and give a 'fake' perfect diamagnetization signal when the magnetic field is applied along the c-axis. This model may explain the phenomenon that the superconducting volume fraction is always large under a magnetic field along the *c*-axis and small within the *ab*-plane, as shown in the inset figure 3(a). Another possibility is the development of a pseudogap [37] at around 50 K. Once the pseudogap is developed at a relatively high temperature, the entropy loss will be a gradual process and take place in a rather wide temperature range, leading to the absence of a jump in heat capacity. In such a case, the jump in heat capacity cannot be detected even if the majority of the layers reach optimal doping.

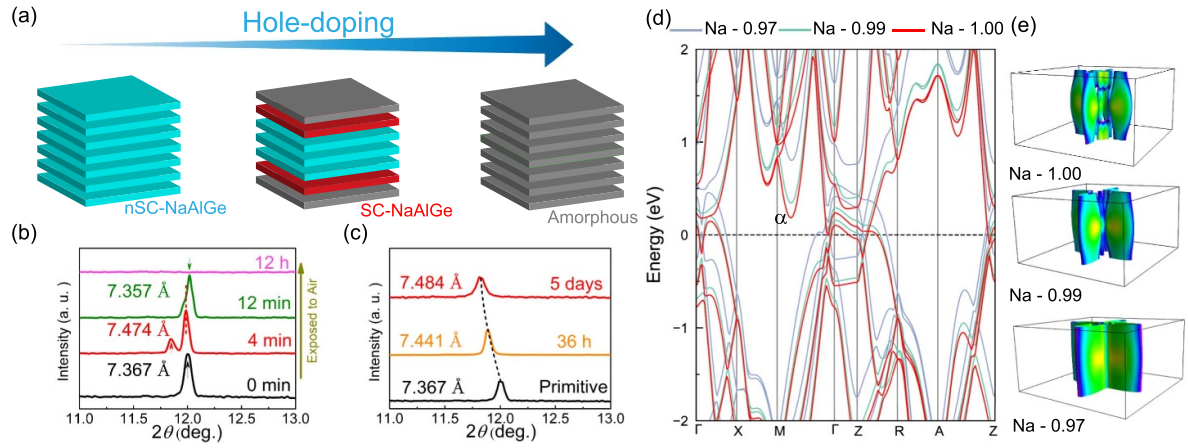

Figure 4. The origin of the superconductivity in NaAlGe single crystal. (a) The diagram of hole-doping induced superconductivity. The cyan/gray layers represent the underdoped/over-doped layer. The red layer represents the hole-doping induced superconducting layer. (b) The (001) peak evolution in a mixture of argon and oxygen. (c) The (001) peak shift before and after soaking in alcohol for time written inside. (d) Electronic band structure of $Na_{1-\delta}AlGe$, $\delta = 0, 0.01, 0.03$. (e) Fermi surface topology of NaAlGe with the variation of Na content. 'The Fermi surface was visualized by FermiSurfer package [36], Copyright © 2014 Mitsuaki Kawamura'.

To further confirm this model, we trace the time evolution of the (001) peak in x-ray diffraction for the sample exposed to air (figure 4(b)) and alcohol treatment (figure 4(c)). When exposed to Ar/O_2, continuous XRD measurements of the (001) peak show an obvious peak shift from 12.00° to 11.83°, which corresponds to a c-axis change from 7.367 Å to 7.474 Å. As the increase of the explosion time, the shifted peak disappeared gradually and became a shoulder of the main (001) peak. After 12 h, the whole crystal was oxidized entirely to be amorphous and no peak was observed. The same situation happened in the alcohol-treated NaAlGe, whose c-axis changed from 7.367 Å to 7.484 Å. Because of the layered structure and the sensitivity of Na atoms between the Al-Ge layers, the peak shift suggests the loss of Na, which reduces the electric attractions and leads to the expansion of the c-axis. We attribute the superconductivity in alcohol-treated or air-exposed NaAlGe single crystals to hole-doped $Na_{1-\delta}AlGe$ with a slightly larger c-axis. When the loss of Na is large, the lattice will collapse and become amorphous phases without diffraction peaks. We note that Al-Ge granular films with nearly 50% Al have been reported to have a semiconductor/insulator-superconductor transition, with its highest T_c lower than 1.8 K [38–40]. Since no superconductor has been reported in Na-Al and Na-Ge binary compounds, we attribute the observed superconductivity to the hole-doping rather than impurities.

To further elucidate the influence of reduction of Na on the electronic structure and consequently lead to the superconductivity, we resort to DFT calculations. As the loss of the amount of Na is tiny, we performed the calculation under the virtual crystal approximation to reduce the computational resource. Figure 4(d) shows the band structure of $Na_{1-\delta}AlGe$ with $\delta = 0, 0.01, 0.03$. With loss of Na (hole doping), the electron pocket along $\mathbf{\Gamma} - M$ gradually move far away from the Fermi level. Thus, this electron pocket is not responsible for the observed superconductivity, unlike the situation in NaAlSi. Besides, we found that the topological nodal lines below the Fermi level moves above the Fermi level. We attribute the induced superconductivity to a critical doping level with nodal lines exactly at the Fermi level. Because the nodal-line near Fermi level is clear to observe, this speculation calls for further study. Nevertheless, the topology is closely interwoven with superconductivity in the hole-doped NaAlGe, which makes it a promising candidate to realize the much-anticipated topological superconductivity. We calculated the Fermi surface evolution as a function of Na concentrations for NaAlGe and plotted it in figure 4(e). The Fermi surface of NaAlGe consists of four open-orbital quasi-cylinders, four sticks around (0, 0, 0.5), and one stick centered at $\mathbf{\Gamma}$. As the concentration of Na decreases, the Fermi surface topology changes. The four sticks around (0, 0, 0.5) gradually disappears and the stick at $\mathbf{\Gamma}$ becomes a quasi-cylinder. Other four open-orbital cylinders are connected. It means the Fermi surface gradually forms a two-dimensional shape with smaller dispersion along the k_z direction. Such a transition of the Fermi surface topology is possibly related to the emergency of superconductivity for the hole doped NaAlGe.

It should be distinguished that the delicate superconductivity reported here is different from the concept of filamentary superconductivity which has been reported in quasi-one-dimensional superconductors $ZrTe_3$ (low-temperature phase) [41], $HfTe_3$ [42] and several others, such as $La_{2-x}Ba_xCuO_4$[43], $CaFe_2As_2$ [44], $Ba(Fe,Co)_2As_2$ [45], and the widely investigated $K_xFe_{2-y}Se_2$ [46, 47]. In these filamentary superconductors, their superconducting volume fraction cannot be further enhanced because of intrinsic phase separation or the observed superconductivity is merely an interface effect. However, in hole-doping NaAlGe, not only zero resistance state but also large diamagnetic drop can be observed. If the loss of Na can be adequately controlled in a gradual and mild manner, bulk superconductivity and thus a jump in heat capacity can be anticipated.

4. Conclusion

In conclusion, we report the discovery of delicate superconductivity in slightly hole-doped NaAlGe single crystals with T_c ranging from 1.8 K to 3.3 K. Hole-doping is realized by moderate oxidation or alcohol treatment. The over 100% superconducting shielding fraction contradicts the lack of a thermodynamic jump in heat capacity, which inspires us to propose a sandwich structure to well explain all the observed phenomena. The construction of a quantitative superconducting phase diagram in NaAlGe, as well as the explanation of the differences between it and its isostructural compound NaAlSi, merits further investigation. Our findings suggest that NaAlGe is an excellent platform with enhanced spin–orbit coupling strength than NaAlSi to study the relationship between the modulated superconductivity and nodal lines on the Fermi surface.

Data availability statement

The data that support the findings of this study are available upon reasonable request from the authors.

Acknowledgments

This work is financially supported by National Key Research and Development Program of China (Grants No. 2017YFA0304700 and 2021YFA1401800) and the MoST-Strategic International Cooperation in Science, Technology and Innovation Key Program (No. 2018YFE0202600).

Note

During the preparation of the manuscript, we noticed that T Yamada *et al* also used Na-Ga flux to obtain the NaAlGe single crystals [37]. While they are focusing on the intrinsic semiconductor of NaAlGe by evaporating Na flux to avoid oxidation.

ORCID iDs

Shixuan Du https://orcid.org/0000-0001-9323-1307
Tianping Ying https://orcid.org/0000-0001-7665-1270
Jiangang Guo https://orcid.org/0000-0003-3880-3012

References

[1] Fang C, Weng H, Dai X and Fang Z 2016 *Chin. Phys.* B **25** 117106
[2] Kim K, Seo J, Lee E, Ko K T, Kim B, Jang B G, Ok J M, Lee J, Jo Y J and Kang W 2018 *Nat. Mater.* **17** 794–9
[3] Liu E, Sun Y, Kumar N, Muechler L, Sun A, Jiao L, Yang S Y, Liu D, Liang A and Xu Q *et al* 2018 *Nat. Phys.* **14** 1125–31
[4] Li P, Koo J, Ning W, Li J, Miao L, Min L, Zhu Y, Wang Y, Alem N and Liu C X *et al* 2020 *Nat. Commun.* **11** 1–8
[5] Ali M N, Gibson Q D, Klimczuk T and Cava R J 2014 *Phys. Rev.* B **89** 020505
[6] Bian G, Chang T R, Sankar R, Xu S Y, Zheng H, Neupert T, Chiu C K, Huang S M, Chang G and Belopolski I *et al* 2016 *Nat. Commun.* **7** 1–8
[7] Long Y-J, Zhao L-X, Wang P-P, Yang H-X, Li J-Q, Zi H, Ren Z-A, Ren C and Chen G-F 2016 *Chin. Phys. Lett.* **33** 037401
[8] Guan S-Y, Chen P-J, Chu M-W, Sankar R, Chou F, Jeng H-T, Chang C-S and Chuang T-M 2016 *Sci. Adv.* **2** e1600894
[9] Wang M, Xu Y, He L, Zhang J, Hong X, Cai P, Wang Z, Dong J and Li S 2016 *Phys. Rev.* B **93** 020503
[10] Kuroiwa S, Kawashima H, Kinoshita H, Okabe H and Akimitsu J 2007 *Physica* C **466** 11–15
[11] Yamada T, Hirai D, Yamane H and Hiroi Z 2021 *J. Phys. Soc. Japan* **90** 034710
[12] Jin L, Zhang X, He T, Meng W, Dai X and Liu G 2019 *J. Mater. Chem.* C **7** 10694–9
[13] Yi X, Li W, Li Z, Zhou P, Ma Z and Sun L 2019 *J. Mater. Chem.* C **7** 15375–81
[14] Muechler L, Guguchia Z, Orain J-C, Nuss J, Schoop L M, Thomale R and Von Rohr F O 2019 *APL Mater.* **7** 121103
[15] Song C, Jin L, Song P, Rong H, Zhu W, Liang B, Cui S, Sun Z, Zhao L and Shi Y 2022 *Phys. Rev.* B **105** L161104
[16] Tapp J H, Tang Z, Lv B, Sasmal K, Lorenz B, Chu P C W and Guloy A M 2008 *Phys. Rev.* B **78** 060505
[17] Deng Z, Wang X, Liu Q, Zhang S, Lv Y, Zhu J, Yu R and Jin C 2009 *Europhys. Lett.* **87** 37004
[18] Rhee H, Banerjee S, Ylvisaker E and Pickett W 2010 *Phys. Rev.* B **81** 245114
[19] Schoop L, Müchler L, Schmitt J, Ksenofontov V, Medvedev S, Nuss J, Casper F, Jansen M, Cava R J and Felser C 2012 *Phys. Rev.* B **86** 174522
[20] Hirai D, Ikenobe T, Yamada T, Yamane H and Hiroi Z 2022 *J. Phys. Soc. Japan* **91** 024702
[21] Wang X, Ding G, Cheng Z, Surucu G, Wang X-L and Yang T 2020 *J. Adv. Res.* **23** 95–100
[22] Song Y, Ying T, Chen X, Han X, Wu X, Schnyder A P, Huang Y, Guo J-G and Chen X 2021 *Phys. Rev. Lett.* **127** 237001
[23] Chen X, Zhan X, Wang X, Deng J, Liu X-B, Chen X, Guo J-G and Chen X 2021 *Chin. Phys. Lett.* **38** 057402
[24] Yang Y, Fan W, Zhang Q, Chen Z, Chen X, Ying T, Wu X, Yang X, Meng F and Li G *et al* 2021 *Chin. Phys. Lett.* **38** 127102
[25] Rodríguez-Carvajal J 1993 *Phys. B: Condens. Matter* **192** 55–69
[26] Kresse G and Furthmüller J 1996 *Comput. Mater. Sci.* **6** 15–50
[27] Perdew J P, Burke K and Ernzerhof M 1996 *Phys. Rev. Lett.* **77** 3865
[28] Monkhorst H J and Pack J D 1976 *Phys. Rev.* B **13** 5188
[29] Allahyari Z and Oganov A R 2020 *J. Phys. Chem.* C **124** 23867–78
[30] Uji S, Konoike T, Hattori Y, Terashima T, Oguchi T, Yamada T, Hirai D and Hiroi Z 2022 *Phys. Rev.* B **105** 235103
[31] Micnas R, Ranninger J and Robaszkiewicz S 1990 *Rev. Mod. Phys.* **62** 113–71
[32] Kitazawa K, Nagano T, Nakayama Y, Tomioka Y and Kishio K 1993 *Appl. Supercond.* **1** 567–79
[33] Sei R, Kitani S, Fukumura T, Kawaji H and Hasegawa T 2016 *J. Am. Chem. Soc.* **138** 11085–8
[34] Carnicom E M, Xie W, Yang Z, Górnicka K, Kong T, Klimczuk T and Cava R J 2019 *Chem. Mater.* **31** 2164–73
[35] Correa L E, Ferreira P P, de Faria L R, Dorini T T, da Luz M S, Fisk Z, Torikachvili M S, Eleno L T F and Machado A J S 2022 *J. Alloys Compd.* **907** 164477
[36] Kawamura M 2019 *Comput. Phys. Commun.* **239** 197–203
[37] Yamada T, Hirai D, Oguchi T, Yamane H and Hiroi Z 2022 (arXiv:2206.04226) [cond-mat.mtrl-sci]

[38] Shapira Y and Deutscher G 1983 *Phys. Rev.* B **27** 4463
[39] Gerber A, Milner A, Deutscher G, Karpovsky M and Gladkikh A 1997 *Phys. Rev. Lett.* **78** 4277
[40] Eytan G, Zaken E, Rosenbaum R, McLachlan D and Albers A 1994 *Physica* B **194** 2419–20
[41] Nakajima H, Nomura K and Sambongi T 1986 Anisotropic superconducting transition in $ZrTe_3$ *Proc. Yamada Conf. XV on Physics and Chemistry of Quasi One-Dimensional Conductors* (Elsevier) pp 240–2
[42] Li J, Peng J, Zhang S and Chen G 2017 *Phys. Rev.* B **96** 174510
[43] Moodenbaugh A, Xu Y, Suenaga M, Folkerts T and Shelton R 1988 *Phys. Rev.* B **38** 4596
[44] Xiao H, Hu T, Dioguardi A, Shockley A, Crocker J, Nisson D, Viskadourakis Z, Tee X, Radulov I and Almasan C *et al* 2012 *Phys. Rev.* B **85** 024530
[45] Xiao H, Hu T, He S, Shen B, Zhang W, Xu B, He K, Han J, Singh Y and Wen H *et al* 2012 *Phys. Rev.* B **86** 064521
[46] Guo J, Jin S, Wang G, Wang S, Zhu K, Zhou T, He M and Chen X 2010 *Phys. Rev.* B **82** 180520
[47] Ding X, Fang D, Wang Z, Yang H, Liu J, Deng Q, Ma G, Meng C, Hu Y and Wen H H 2013 *Nat. Commun.* **4** 1–7